J. Fluid Mech. (1983), *vol.* 132, *pp.* 257–270
Printed in Great Britain

Shock diffraction in channels with 90° bends

By D. H. EDWARDS,
Department of Physics, University College of Wales, Penglais, Aberystwyth

P. FEARNLEY
B.P. Research Centre, Sunbury-on-Thames, Middlesex

AND M. A. NETTLETON
Central Electricity Research Laboratories, Kelvin Avenue, Leatherhead, Surrey, KT22 7SE

A study has been made of how initially planar shocks in air propagate around 90° bends in channels of nearly rectangular cross-section. In shallow bends for which the radius of curvature R is much greater than the radius r of the channel, the shock recovers from a highly curved profile at the start of the bend to regain planarity towards the end of the bend. This occurs on account of the acceleration of the triple point across the channel following its interaction with the expansion waves generated at the convex wall. In sharp bends the shock profiles retain their pronounced curvature for some distance downstream of the bend.

At the start of a shallow bend ($R/r \approx 6$) the shock at the concave wall, initial Mach number M_0, accelerates to $M_w = 1.15M_0$ and remains at this value until towards the end of the bend it begins to attenuate. At the convex wall, shocks of $M_0 > 1.7$ attenuate to $M_w = 0.7M_0$ and propagate at this value for some distance around the bend. In the early stages of a sharper bend ($R/r \approx 3$) the shock at the concave wall strengthens to $M_w = 1.3M_0$, remaining at this value for some distance downstream of the bend. At the convex wall the shock decelerates to $0.6M_0$.

Whitham's (1974) ray theory is shown to predict with reasonable accuracy the Mach numbers of the wall shocks at both surfaces for both bends tested and the range of incident shock velocities used, $1.2 < M_0 < 3$. The agreement between the theory and experimental results is particularly close for stronger shocks propagating along the inner bend. Predictions from 3-shock theory (Courant & Friedrichs 1948) of the Mach number at the outer wall are consistently higher than those from Whitham's analysis. In turn, the latter tends to slightly overestimate the strength of the wall shock.

A model is developed, based on an extension of Whitham's analysis, and is shown to predict the length of the Mach stem produced by shocks of $M_0 > 2$ over the initial stages of the bend.

1. Introduction

Although the diffraction of shock waves on isolated curved surfaces has been studied in detail (Whitham 1974), little is known about the interactions of the wave systems set up at the convex and concave surfaces of a bend in a channel. The pioneering investigation of Hide & Millar (1956) examined the relationship between the radius of curvature R of a bend in a channel of rectangular cross-section and its width $2r$ (figure 1), required for a planar front to propagate through the bend at constant angular velocity. Fearnley & Nettleton (1983) extended this study to the

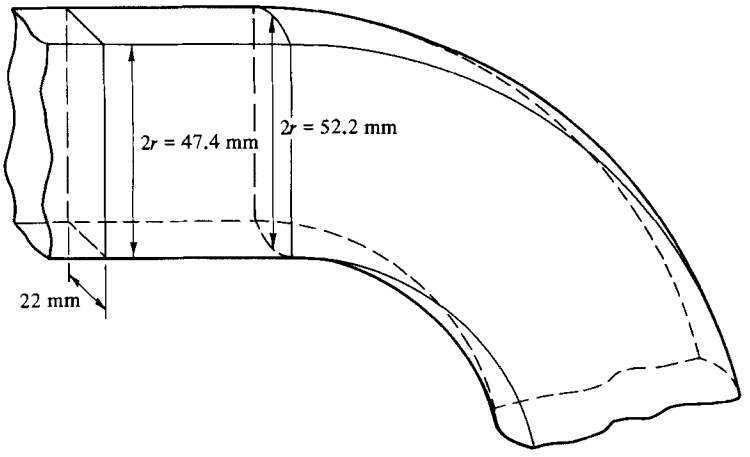

FIGURE 1. Gradual change in cross-section at the start of the bends.

decay in shock strength downstream of 90° bends in channels of rectangular cross-section. In addition, they gave a qualitative description of how the shock profiles varied within the bend. Finally, Edwards *et al.* (1981) have interpreted soot track records, written by Mach triple points on walls by detonations in mixtures of acetylene and oxygen travelling around similarly dimensioned bends, in terms of the profiles of non-reactive shocks.

There were two principal objectives of the present experiments. The first of these was to investigate whether shock-focusing effects might occur in a bend of circular cross-section. Consequently, the two narrower walls of the bend were modified to introduce a degree of curvature in the cross-section. Unfortunately, the error limits on the limited number of previous measurements of velocities of wall shocks (Fearnley & Nettleton 1983) were too wide to permit meaningful comparisons between channels of rectangular and partly curved cross-section. However, there were significant differences in the trajectories of the triple points across the two forms of cross-section. These are described in §3.3.

The second objective was to improve upon the accuracy of the measurements of velocity of the shock within the bend itself. This was achieved by the use of a multispark light source in conjunction with the schlieren system recording the shock profiles. With this it was possible to obtain up to five profiles, and hence four velocities at each wall, from a single experiment. Consequently, it was possible to reduce the scatter in the experimental results, introduced by slight variations in the velocity of the shock incident on the bend. The gradual change in cross-section of the inlet to the bend was sufficiently small, less than 0.5%, to allow a valid comparison of the velocities measured in bends of $R = 75$ and 150 mm with standard 3-shock theory (Courant & Friedrichs 1948) and with Whitham's (1974) ray theory. The latter is shown to produce a satisfactory description of the enhancement of the Mach number at the outer wall and its attenuation at the inner wall up to the point at which the reflected wave interacts with the expansion wave. The wall shocks were observed to propagate at a constant velocity for some distance downstream of this conjunction.

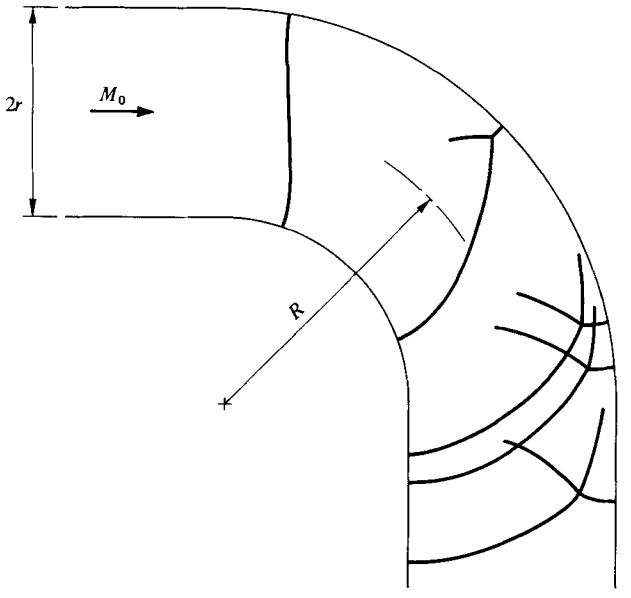

FIGURE 2. Shock profiles for $m_0 = 2.8$, $\gamma = 1.4$ in bend 1 ($R = 75$ mm, $r = 26.1$ mm).

2. Experimental

Two bends, with radii of curvature 75 and 150 mm, were used in the present experiments. They were constructed from aluminium blocks which were sandwiched between two schlieren-quality glass windows. The rectangular cross-section of the inlet duct, of 22×47.4 mm, was gradually contoured at the start of the bend to produce a smooth transition to a partly curved cross-section, by machining the 22 mm walls to a radius of curvature of 26.1 mm (see figure 1). Thus the cross-sectional area of the inlet channel, 1043 mm^2, increased smoothly to a maximum of 1096 mm^2 at a distance of approximately $\frac{1}{2}r$ into the bend. Such a change in area should result in only very slight attenuation in the velocity of the shock. For instance, Chisnell's (1957) relationship between the Mach number of the shock and the area indicates that a shock of velocity $M_0 = 2.90$ incident on the bend should decay to $M = 2.87$.

Planar shocks were generated principally in air, and on occasion in argon, in a 3 m length of the inlet channel, using either air or helium as the high-pressure gas. A series of pressure transducers were positioned towards the end of the channel, in order to correct the velocity of the shock incident on the bend for possible retardation in the channel. Any such corrections amounted to less than 0.1 % of M_0. The signal from the pressure gauge closest to the bend was used to fire the light source after a predetermined delay. The schlieren system was of conventional design, with 300 mm diameter mirrors to cover as much of the bend as possible.

3. Results

3.1. *Schlieren records of shock profiles*

A selection of shock profiles, produced by an $M_0 = 2.8$ shock in air diffracting round bend 1 ($R = 85$ mm), is illustrated in figure 2. The shock does not recover to a planar front within the bend itself for the range tested, $2.8 > M_0 > 1.2$. The trajectory of the triple point shown is typical of shocks with $M_0 > 2$. Weaker shocks result in similar

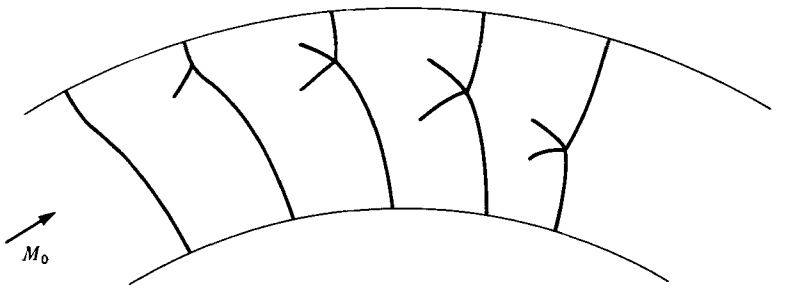

FIGURE 3. Shock profiles for $M_0 = 2.9$, $\gamma = 1.4$ in bend 2 ($R = 150$ mm, $r = 26.1$ mm).

curvature of the incident shock within the bend. However, the path of the triple point is modified such that it travels a much shorter distance towards the inner wall. The Mach stem continues gradually to lengthen for radial angles travelled ϕ of up to approximately 40°. The stem then rapidly contracts, producing a transition to regular reflection at $\phi = \phi_{\text{crit}}$ for which $45° < \phi_{\text{crit}} < 50°$, in similar fashion to diffraction on isolated concave surfaces (Gvozdeva, Lagutov & Fokeev 1979; Itoh & Itaya 1980).

Some caution is necessary in comparing results from isolated surfaces with those from channels. The usual criterion for isolated surfaces involves the critical angle for transition α_{crit}, defined as the angle between the incident shock and the tangent to the surface at the transition, or $90° - \phi_{\text{crit}}$. For weak shocks α_{crit} is strongly influenced by M_0. In the channel, the incident shock has decayed to a Mach number below M_0 before transition occurs. Again, the pronounced curvature of the incident shock in the channel calls into question the accuracy of the simple relationship between α_{crit} and ϕ_{crit} applicable to isolated curve surfaces. Notwithstanding these cautionary remarks, Itoh & Itaya (1980) give, for a curved surface, $70° > \alpha_{\text{crit}} > 50°$ for $1.2 < M_0 < 2$, not greatly different from the present results.

Figure 3 is a similar composite illustration for a shock with $M_0 = 2.9$ in air diffracting around the midportion of bend 2 ($R = 150$ mm). Here the curvature of the trajectory of the triple point is much tighter than that of the bend itself. Consequently, for shocks with $M_0 > 2$, recovery to a planar front occurs within the bend itself. Weaker shocks result in the transition from Mach to regular reflection occurring at $\phi_{\text{crit}} \approx 60°$, and both main and reflected waves retain their curvature throughout the bend.

3.2. *Velocities of wall shocks*

Velocities U_s of the wall shocks were obtained from records, such as those shown in figures 2 and 3, from distances the shocks travelled around inner and outer walls in the accurately preset intervals between sparks, and converted to Mach numbers ($M_w = U_s/a$), using the value of sound speed a appropriate to the temperature of the gas ahead of the shock. In order to incorporate the results of a number of experiments in which there were slight but unavoidable variations in the velocity of the shock incident on the bend, the results have been normalized by division by M_0. Because the results extended beyond the curved portion of the outer wall, they are plotted in terms of hydraulic diameters ($4 \times$ cross-sectional area $\div$ perimeter) traversed, rather than in terms of radial angle. Again, the ratios M_w/M_0 have been plotted at the mean distance from the start of the curvature of the bend of the two profiles used in obtaining the velocity.

Figures 4–6 show how the Mach numbers of the wall shocks vary around bend 1 for shocks of $M_0 = 1.7$, 2.1 and 2.7. Included in figure 6 are the limits of experimental

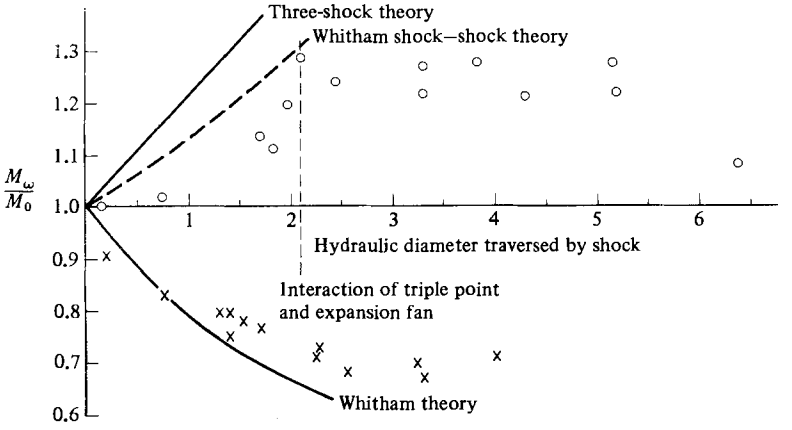

FIGURE 4. Variation in velocity of wall shocks during propagation through bend 1, $M_0 = 1.7$, $\gamma = 1.4$.

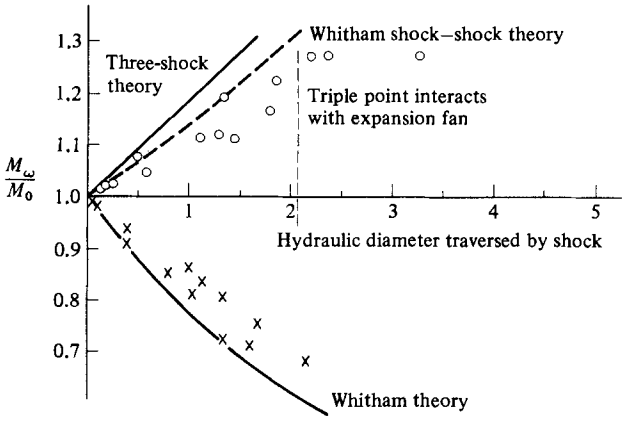

FIGURE 5. Shock velocity as a function of distance travelled in bend 1, $M_0 = 2.1$, $\gamma = 1.4$.

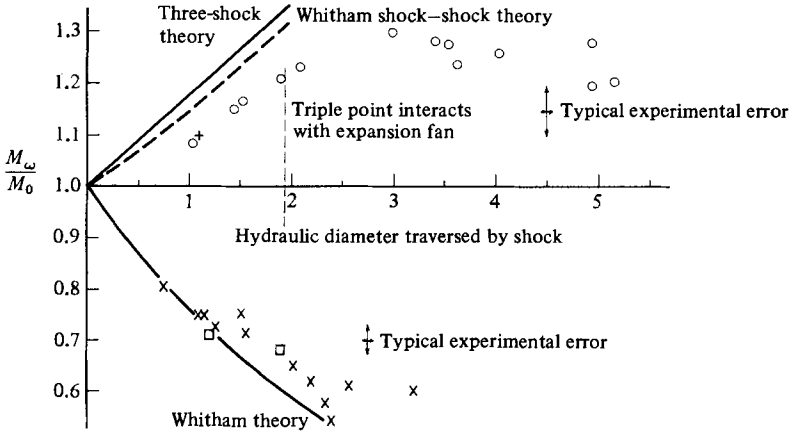

FIGURE 6. Influence of distance travelled on velocity of wall shocks in bend 1, $M_0 = 2.7$, $\gamma = 1.4$: ○, ×, curved walls; □, +, straight walls.

error, estimated from possible errors in the measurements of the time intervals between sparks and of distances travelled by the wall shocks. The trajectory of the head of the expansion wave generated at the start of the inner wall has been calculated following Skews' (1967) analysis. The positions at which the triple point interacts with the head of the expansion wave, derived from these calculations, are given in figures 4–6.

The Mach number of the shock incident on the bend has no effect on the maximum value of M_w/M_0 at the concave wall of bend 1. The ratio increases to $M_w/M_0 = 1.3$ at approximately 2 diameters into the bend, corresponding to the position at which the interaction between triple point and expansion wave occurs. The wall-shock Mach number then remains constant at $1.3M_0$ for a further 3 diameters, by which stage the wall shock has travelled some distance downstream of the bend. Thus it appears that, within the bend itself, the effects of the expansion fan in slowly attenuating the strength of the wall shock are counterbalanced by the effects of the curvature of the bend in enhancing the strength of the shock. Pronounced attenuation first occurs between 5 and 6 diameters downstream of the start of the bend, with M_w falling to $1.1M_0$ at just over 6 diameters (figure 4).

At the convex wall of bend 1, shocks of $M_0 = 2.7$ attenuate to a Mach-number ratio of about 0.6, and weaker shocks, $M_0 \leqslant 2.1$, fall to about $0.7M_0$, as they approach the end of the bend at about 2 hydraulic diameters. The results for the weaker shocks indicate that the Mach number remains constant for a further diameter, at which point the shock at the inner wall has travelled downstream of the bend.

Figures 7–9 show the Mach numbers of wall shocks in bend 2, produced by shocks of $M_0 = 1.2$, 1.9 and 2.9. Although there is some similarity in the general shapes of the plots from both bends, the following features differ significantly. Enhancement of the shock at the outer wall of bend 2 is considerably less than that which occurs in bend 1, with M_w increasing to a maximum value of $1.15M_0$. Furthermore, M_w continues to increase for approximately a further diameter after the interaction of the triple point and the expansion fan, and the maximum value of M_w occurs at just over 3 diameters from the start of the bend. There is also some suggestion that the distance around the bend for which M_w remains constant varies with M_0. With $M_0 = 1.2$ (figure 7), M_w is constant up to 7 diameters, whereas, for $M_0 \leqslant 2.9$, M_w starts to fall at a distance not exceeding 5.5 diameters. Again, the attenuation of the shock at the inner wall is less in bend 2 than in bend 1. A shock with $M_0 = 1.2$ decays to approach a sound wave at approximately 4 diameters (figure 7). The stronger shocks decay to $0.7M_0$ at between 3.5 and 4 diameters. Figure 8 shows how the Mach number of the shock at the inner wall starts to increase again, at between 5 and 6 diameters, as the triple point reaches the inner wall.

3.3. *Growth of Mach stem*

Fearnley & Nettleton (1983) have described the profiles produced by shocks diffracting around 90° bends in channels of rectangular cross-section, and have given some estimates of the Mach number of the wall shock at the early stages of the inner and outer walls of the bend. Although these were subject to a rather large range of experimental error, their comparison with the present results, shown in figures 6, 8 and 9, suggests that the change in cross-section of the bend had little effect on the Mach number of the wall shocks. However, there were significant differences in the trajectory of the triple point. Figure 10 illustrates this effect for the two versions of bend 2, with the triple point advancing across the channel at a much earlier stage

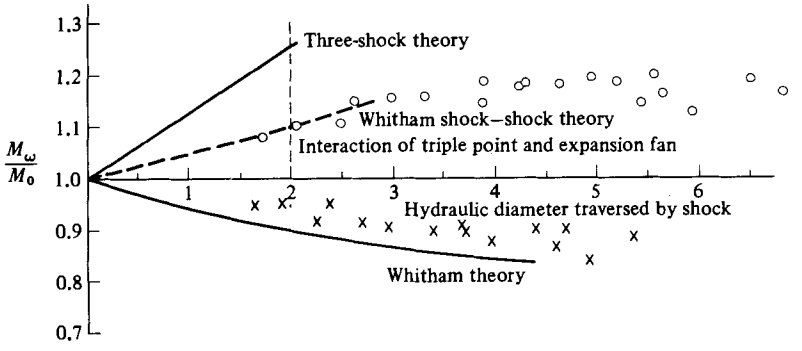

FIGURE 7. Variation in the velocity of wall shocks during propagation through bend 2, $M_0 = 1.2$, $\gamma = 1.4$.

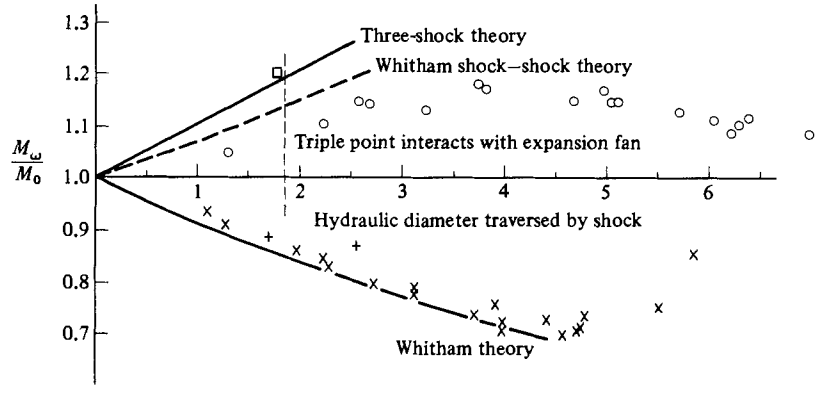

FIGURE 8. Influence of distance travelled on velocity of wall shocks in bend 2, $M_0 = 1.9$, $\gamma = 1.4$: ○, ×, curved-wall channel; □, +, flat-walled channel.

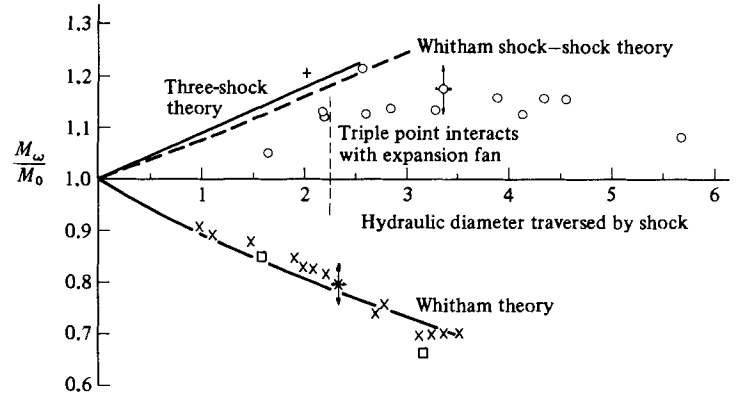

FIGURE 9. Influence of distance travelled on velocity of wall shocks in bend 2, $M_0 = 2.9$, $\gamma = 1.4$: ○, ×, curved-walled channel; □, +, flat-walled channel.

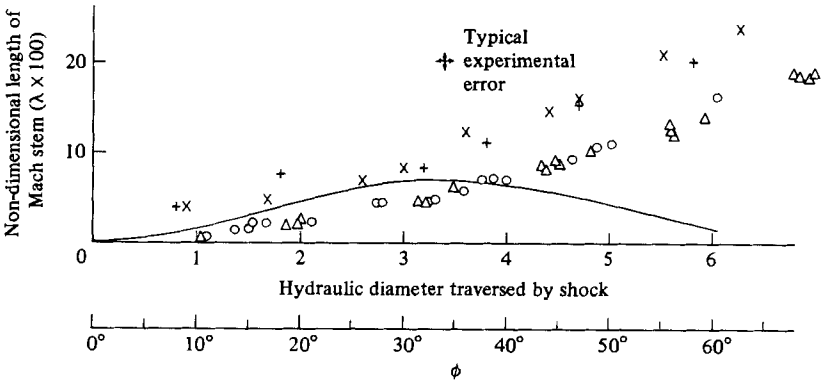

FIGURE 10. Growth of Mach stem in bend 2. Curved walls; ○, $M_0 = 2.9$, △, 1.9. Flat walls: +, $M_0 = 2.1$; ×, 3.0.

in the channel of rectangular cross-section. The differences in trajectories were even more pronounced in the rectangular and non-rectangular cross-section versions of bend 1.

There are a number of factors which may contribute to the difference in trajectories. Chisnell's (1957) relationship between the Mach number of the shock averaged over its periphery and its area indicates that the overall effect of the increased area of the non-rectangular channel should be a reduction of only about 1 % in Mach number. However, the change in the Mach number of the shock will be localized to close to the walls at the start of the modified cross-section, resulting in a greater degree of attenuation of the wall shocks there. Nonetheless, whereas the experimental trajectories increasingly diverge with distance travelled in the two cross-sections, Chisnell's treatment should become more satisfactory. The method used to introduce gradually the change in cross-section may be of more import. At the concave side, the curvature was introduced at the outer walls, so that diffraction occurred there first, travelling towards the vertical plane of symmetry. At the convex side the curvature started at the plane of symmetry, with diffraction travelling out to the vertical walls (figure 1). Thus, both wall shocks and the reflected front will be curved between the walls of 22 mm width. In addition to attenuation caused by the increased area of the shocks, the change in sound and particle velocity of the gas into which the reflected wave is propagating may be a further factor.

4. Discussion

4.1. *Main features of shock diffraction in a bend in a channel*

Before discussing available theories of shock diffraction, it may be useful to summarize the various processes which modify the shape of the shock as it travels around a bend in a channel. Figures 11 (*a*, *b*) show typical profiles produced by strong shocks, say $M_0 > 2$, at the start and approaching the end of a bend with $R = 3r$. Included in the sketches are particle paths immediately behind the shock front.

As the shock enters the bend it is subjected to the effects of an expansion wave centred on O on the convex wall. The angle in between the head of this wave, OH, and the original direction of the wall, OX, is a function of M_0, but for strong shocks can be taken as m_0, where $28° > m_0 > 23°$ (Skews 1967). The area associated with EH of the shock profile in figure 11 (*a*) is subjected to the combined effects of the

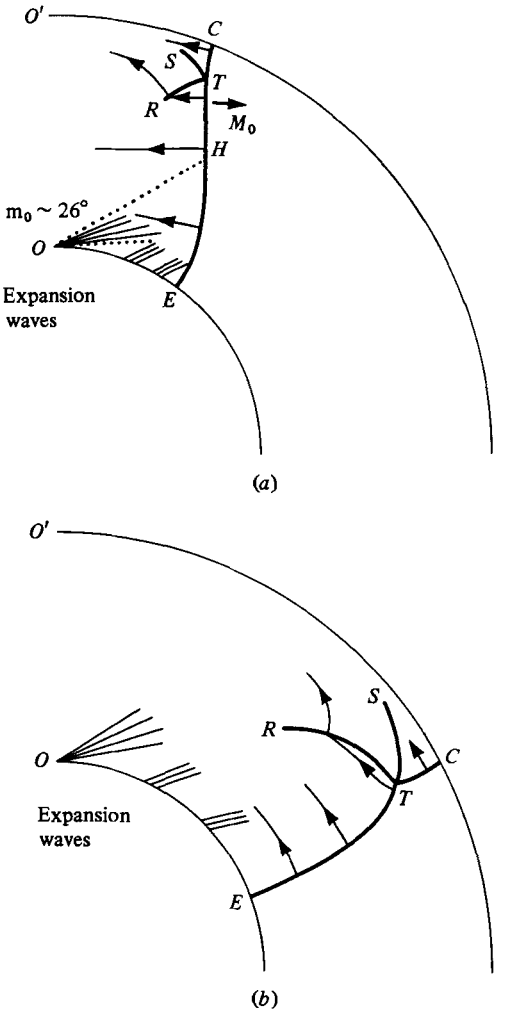

FIGURE 11. Interaction of shock and expansion waves and resultant particle paths in a sharp bend: *CT*, Mach stem; *TS*, slipstream; *TR*, reflected shock; *TH*, incident shock; *OH*, head of expansion front centred at *O*; *EH*, *ET*, attenuating shock profile.

expansion centred on *O* and the diffuse expansion waves originating along the curve *OE*. Between *H* and the triple point *T* a portion of the front continues to propagate at M_0. Because the reflected shock *TR* curves sharply towards the convex wall, a significant portion of the gas is compressed by a combination of the incident front travelling at M_0 and the reflected front. The Mach stem *TC* exhibits a shallow curvature, as it increases in length along the concave wall *O'C*.

Figure 11 (*b*) shows the shock further downstream in the bend, when the expansion waves have travelled across to the outer wall, attenuating the portion of the profile originally propagating at M_0 and interacting with the triple point, before they reflect from the outer wall. At this stage the attenuating profile exhibits pronounced curvature close to the triple point. This results in the particle paths being directed towards the inner wall, so that the reflected wave starts to be convected across the channel. Again, as the expansion waves interact with the Mach stem it becomes markedly more curved.

4.2. *Theoretical treatments of shock diffraction*

There are two principal analyses of the behaviour of shocks on curved surfaces. The first, applying to concave curves, is three-shock theory (Courant & Friedrichs 1948), and the second, which can be used at either convex or concave surfaces, is Whitham's (1974) ray theory. A brief description of these, especially of the assumptions inherent in their derivation, should clarify the features of shock diffraction in a channel to which each analysis is most appropriate. It should be noted that attempts to validate the theories by previous experiments on isolated curved surfaces have satisfied the theoretical requirement of the continuous existence of a portion of the incident shock. The present experimental results are not covered by existing theories at points downstream of the interaction of the expansion head and triple point.

Three-shock theory is based on the premise of Mach reflection occurring at small wall angles and regular reflection at larger angles. It involves matching pressures across the slipstream in the flow created by both incident and reflected shocks with those in the flow created by the Mach stem. In order to do this, all shocks are considered to be straight and the Mach stem to propagate orthogonally to the wall. In the present experiments the reflected shock is invariably curved, possibly in both horizontal and vertical planes, and the curvature increases with distance from the triple point. Again, the Mach stem, especially the portion close to an isolated wall, is generally believed to be curved (Whitham 1974). With the Mach stem propagating at right angles to the wall, this should lead to the model overestimating the strength of the wall shock. Even larger errors might be expected on account of the pronounced curvature of the portion of the Mach stem close to the triple point, following its interaction with the expansion waves in the channel.

More recently, Whitham (1974) extended the methods of characteristics to deal with the propagation of a curved portion of shock front through a tube of varying cross-section, bounded by rays orthogonal to the front. In order to relate the changing area of the front with Mach number, Whitham's method incorporates the Chester–Chisnell (1957) theory. This has been shown to perform well in describing the early stages of the decay of both slowly expanding (Nettleton 1973) and rapidly expanding fronts (Sloan & Nettleton 1975, 1978). The rapidly changing area of shock at the concave wall, where convergence of the characteristic paths is identified with the formation of the reflected shock, probably imposes a much more severe test of the theory than does the convex corner.

Lighthill (1949) produced an exact analysis of shock diffraction around a convex corner. It is based on a self-similarity solution in terms of non-dimensional distances in (x, y)-coordinates with a linearized flow field behind the front. However, linearization is only possible for small corner angles, so that the Whitham analysis is the only one of general applicability. Fortunately, Skews (1967) has shown that the Whitham theory is reasonably satisfactory for convex corners and generally produces improving agreement between theory and experiment the stronger the incident shock. This improvement in agreement is to be expected in that Whitham's treatment tends to concentrate disturbances originating from the corner and propagating into the flow field behind the front, whereas the Lighthill analysis shows this to be true only for strong shocks.

To sum up, the general applicability of the Whitham analysis and its satisfactory performance in describing propagation over surfaces of both expansion (Skews 1967) and compression (Henderson 1980) makes it an obvious choice with which to compare the present experimental results. It has presently been applied using the procedure

first outlined by Bryson & Gross (1961). In order to produce an assessment of the probably magnitude of differences between predictions from available models, wall shock velocities have also been calculated using three-shock theory.

4.3. *Variation in velocity of wall shock during propagation around bends*

For the convex surfaces of both bends and for distances up to twice that at which attenuation of the original shock starts, the Whitham analysis gives a good description of the experimental results. As would be expected from the simplifications in the analysis, the agreement between prediction and experiment improves with increasing Mach number of the shock incident on the bend. There is also some indication that Whitham's treatment is more accurate for shallow bends. Thus, there is a considerable improvement in the predicted results for bend 1, when M_0 increases from 2.1 (figure 5) to 2.7 (figure 6), whereas, for bend 2, prediction and experiment are in excellent accord for a lower value of velocity of incident shock, $M_0 = 1.9$ (figure 8).

Three-shock theory predicts considerably stronger shocks on the outer wall than does Whitham's analysis. The difference between the theories increases with decreasing values of M_0 (see figures 4–6). Whitham's analysis closely describes the experimental results for weak shocks in shallow bends (see figure 7). However, for stronger shocks and sharper bends, it too tends to overestimate the Mach numbers of the wall shocks. This is to be expected in view of the severe test imposed in applying the Chester–Chisnell relationship to strong shocks in sharp contractions in area.

The distances around the bend over which the Whitham treatment continues to produce tolerable descriptions of the Mach numbers of the wall shocks are of interest. At the convex walls of both bends the theory continues to perform satisfactorily up to close to the end of the bend, where the experimental results remain constant. The observation that the analysis can be used to predict Mach numbers along the length of the inner wall of both bends is somewhat surprising. Towards the end of the shallower bend the shock at the inner wall will have been subject to the effects of both the expansion waves originating from that wall and their reflections from the outer wall. However, the implication of the relatively slow weakening of a wall shock by an expansion fan has some supporting experimental evidence (Sloan & Nettleton 1975, 1978). Again, the Whitham treatment can be used along the length of the outer wall of the sharper bend, as the observed region of constant Mach number corresponds reasonably closely with the distance at which the triple point interacts with the head of the expansion fan. However, the choice of a signpost, marking departure between theory and experiment, presents a problem in the case of the outer walls of shallow bends. Here the wall shock is observed to continue to increase in Mach number some distance downstream of the interaction between the triple point and expansion fan.

4.4. *Trajectory of the triple point*

An analysis of the growth of Mach stems on shocks propagating around bends joined smoothly to the inlet channel is given in the appendix. Briefly, it gives the length λ of the Mach stem in terms of the radial angle ϕ travelled by the wall shock, for strong shocks as $\lambda = \cos^n\phi\,(1-\cos\phi)$ for $\phi \leqslant \cos^{-1}[(R-r)/(R+r)]$. Itoh & Itaya (1980) have extended Bryson & Gross's (1961) analysis and produced a similar derivation for shocks in bends in which the straight channel makes an abrupt transition into the bend at angle of $2\pi-\theta$. Figure 10 illustrates the results obtained from the present theory for shocks with $M_0 \geqslant 2$ in both versions of bend 2. Although the analysis is more appropriate to the flat-walled version of the bend, it adequately

predicts the trend of the experimental results for $\phi \leqslant 30°$ for both versions of the bend. This is approximately twice the angle at which the interaction between the triple point and the expansion fan from the opposite wall starts. For $\phi > 30°$ the theory predicts shrinking of the Mach stem, to produce a transition back to regular reflection at about $\phi = 70°$, whereas the interaction of the triple point and expansion fan leads to the continued growth of the stem.

In order to extend the analysis to $\phi > \cos^{-1}[R-r/(R+r)]$, a description of the flow field (particle and sound velocities) behind the attenuating front together with the shape of the reflected front are required. Whilst it is probably possible to compute the shape of the reflected shock produced by a concave-curved surface (see e.g. for wedges, Ben-Dor & Glass 1979), the flowfield behind the attenuating shock presents a major problem. This is because of the continuous nature of the modifications to the flowfield, imposed by the expansion fan originating from a curved surface.

5. Conclusions

The following generalizations may be drawn on the diffraction of shocks as they propagate around 90° bends in channels.

(i) The velocity ratios associated with the wall shocks at both outer and inner bends were influenced by the sharpness of the bend. In the present study the maximum ratio observed at the concave wall was $M_w/M_0 = 1.3$. Likewise the minimum ratio at the convex wall was $M_w/M_0 = 0.6$. These occurred with the sharper of the two bends tested.

(ii) Following the regions in which the ratios of Mach numbers increased at the outer wall and fell at the inner, the ratios remained constant through most of the remainder of the bend. Thus, the complex interactions of the reflected shock front and expansion fan and the resultant fronts with the walls of the channel, resulting in a stable and planar front, are only completed well downstream of the bend.

(iii) Whitham's ray theory has been shown to predict adequately the enhancement of the wall shock at the outer wall and its attenuation at the inner wall. The agreement between the theory and experiment was closest for the convex surface and improved for the concave surface with increasing velocity of the incident shock.

(iv) An adaptation of Whitham's ray theory describing the growth of the Mach stem has been shown to perform reasonably well for strong ($M_0 > 2$) incident shocks.

P. F. wishes to thank the Central Electricity Generating Board for financial support in the form of a CASE studentship. The authors are grateful to G. B. Whitham, F.R.S., for his helpful comments.

Appendix

Consider a shock of velocity M_0 entering the bend and producing a Mach stem of length λ at an angle ϕ to the centre of curvature (figure 12). Following Whitham's (1974) ray theory, all rays originally passing through TQ pass through the Mach stem, and, normalizing TQ and λ with respect to the lengthscale $R+r$,

$$TQ = 1-(1-\lambda)\cos\phi. \tag{A 1}$$

From the Chester–Chisnell relationship between the Mach number and area of a shock,

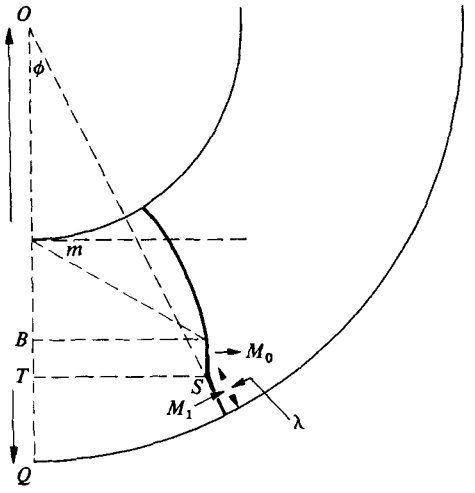

FIGURE 12. Relationship between λ and ϕ in a curved channel.

the ratio of the incident and stem Mach numbers is

$$\frac{M_0}{M_1} = \left[\frac{1-(1-\lambda)\cos\phi}{\lambda}\right]^{-1/n}. \tag{A 2}$$

For infinite M_0, $n = 5.074$ for a gas of $\gamma = 1.40$ and 4.436 for a gas of $\gamma = 1.667$.

Self-similarity considerations give the α-coordinate of the incident shock as

$$\alpha = \frac{x}{M_0} = \frac{ST}{M_0} = \frac{(1-\lambda)\sin\phi}{M_0}. \tag{A 3}$$

As $1/M = |\nabla\alpha| = R^{-1}\partial\alpha/\partial\phi$, (A 2) and (A 3) give

$$\frac{M_0}{M_1} = \frac{1}{R}\frac{\mathrm{d}}{\mathrm{d}\phi}(1-\lambda)\sin\phi. \tag{A 4}$$

Differentiation of (A 4) gives

$$\frac{M_0}{M_1} = \frac{1}{1-\frac{1}{2}\lambda}\left\{(1-\lambda)\cos\phi - \sin\phi\frac{\mathrm{d}\lambda}{\mathrm{d}\phi}\right\} \tag{A 5}$$

Combining (A 4) and (A 5) and rearranging gives

$$\frac{\mathrm{d}\lambda}{\mathrm{d}\phi} = (1-\lambda)\cot\phi - \frac{1-\frac{1}{2}\lambda}{\sin\phi}\left\{\frac{\lambda}{1-(1-\lambda)\cos\phi}\right\}^{1/n}. \tag{A 6}$$

With both $\mathrm{d}\lambda/\mathrm{d}\phi$ and $\lambda \ll 1$, (A 6) simplifies to

$$\lambda = \cos^n\phi(1-\cos\phi). \tag{A 7}$$

Figure 12, showing the head of the expansion wave from the beginning of the convex bend advancing at an angle m, indicates the range of ϕ over which (A 6) and (A 7) should hold. This is from $\phi = 0$ to ϕ at which $BT = 0$, when all of the original shock starts to attenuate. With $TS = aM_0\,\Delta t$, where a is the speed of sound in the gas ahead of the shock, $BT = 0$ when

$$\phi = \cos^{-1}\frac{R-r+aM_0\,\Delta t\tan m}{R+r-\lambda}, \tag{A 8}$$

where R is the radius of curvature of the channel and r is the radius of the channel. With $R-r \gg aM_0 \Delta t \tan m$ and $R+r \ll \lambda$, (A 8) gives

$$\phi_m = \cos^{-1}\frac{R-r}{R+r}. \tag{A 9}$$

REFERENCES

Ben-Dor, G. & Glass, I. I. 1979 Domains and boundaries of non-stationary oblique shock-wave reflexions. Part 1. Diatomic gas. *J. Fluid Mech.* **92**, 459.

Bryson, A. E. & Gross, R. W. F. 1961 Diffraction of strong shocks by cones, cylinders, and spheres. *J. Fluid Mech.* **10**, 1.

Chisnell, R. F. 1957 The motion of a shock wave in a channel, with applications to cylindrical and spherical shock waves. *J. Fluid Mech.* **2**, 286.

Courant, R. & Friedrichs, K. O. 1948 *Supersonic Flow and Shock Waves.* Interscience.

Edwards, D. H., Fearnley, P., Thomas, G. O. & Nettleton, M. A. 1981 Shocks and detonations in channels with 90° bends. *1st Specialists' Meeting (Intl) Combust. Inst.*, p. 431. Section Française du Combust. Inst.

Fearnley, P. & Nettleton, M. A. 1983 Pressures generated by blast waves in channels with 90° bends. Submitted to *Loss Prevention and Safety Promotion Meeting, Inst. Chem. Engng.*

Gvozdeva, L. G., Lagutov, Yu. P. & Fokeev, V. P. 1979 Transition from normal reflection to Mach reflection in the interaction of shock waves with a cylindrical surface. *Sov. Tech. Phys. Lett.* **5**, 334.

Henderson, L. F. 1980 On the Whitham theory of shock-wave diffraction. *J. Fluid Mech.* **99**, 801.

Hide, R. & Millar, W. 1956 A preliminary investigation of shocks in a curved channel. *AERE* GP/R 1918.

Itoh, S. & Itaya, M. 1980 On the transition between regular and Mach reflection. In *Shock Tubes and Waves: Proc. 12th Intl Symp. on Shock Tubes and Waves* (ed. A. Lifshitz & J. Rom), p. 314. Magnes Press, Hebrew University, Jerusalem.

Lighthill, M. J. 1949 The diffraction of blast. 1. *Proc. R. Soc. Lond.* **A198,** 454.

Nettleton, M. A. 1973 Shock attenuation in a 'gradual' area expansion. *J. Fluid Mech.* **60**, 209.

Skews, B. W. 1967 The shape of a diffracting shock wave. *J. Fluid Mech.* **29**, 297.

Sloan, S. A. & Nettleton, M. A. 1975 A model for the decay of the axial shock in a large and abrupt area change. *J. Fluid Mech.* **71**, 769.

Sloan, S. A. & Nettleton, M. A. 1978 A model for the decay of the wall shock in a large and abrupt area change. *J. Fluid Mech.* **88**, 259.

Whitham, G. B. 1974 *Linear and Nonlinear Waves.* Wiley-Interscience.